

# Automatic cell counting for phase-contrast microscopic images based on a combination of Otsu and watershed segmentation method

Yuefei Lin<sup>1</sup>  | Yong Diao<sup>1</sup> | Yongzhao Du<sup>1,2,3</sup> | Jianguang Zhang<sup>1</sup> | Ling Li<sup>1</sup> | Peizhong Liu<sup>1,2,3</sup>

<sup>1</sup>School of Medicine, Huaqiao University, Quanzhou, China

<sup>2</sup>College of Engineering, Huaqiao University, Quanzhou, China

<sup>3</sup>Medical College, Quanzhou, China  
Collaborative Innovation Center for Maternal and Infant Health Service Application Technology, Quanzhou, China

## Correspondence

Peizhong Liu, College of Engineering, Huaqiao University, Quanzhou, China.  
Email: pzliu@hqu.edu.cn

## Funding information

Fujian Provincial Big Data Research Institute of Intelligent Manufacturing; Fujian Provincial Science and Technology Major Project, Grant/Award Number: 2020HZ02014; National Natural Science Foundation of China, Grant/Award Number: 61605048; Promotion Program for Young and Middle-aged Teacher in Science and Technology Research of Huaqiao University, Grant/Award Number: ZQN-PY518; Quanzhou scientific and technological planning projects, Grant/Award Numbers: 2018Z176, 2018C113R, 2019C028R, 2019C029R

Review Editor: Alberto Diaspro

## Abstract

Cell counting plays a vital role in biomedical researches. However, manual cell counting is time-consuming, laborious, and low efficiency and has a high counting error rate problem. An automatic counting approach for HeLa cells of phase-contrast microscopic images is proposed based on the combination of Otsu and watershed segmentation methods to solve the mentioned issues. Firstly, image preprocessing is performed. Secondly, the Otsu method was used to obtain an automatic global optimal threshold for segmentation to achieve batch counting of images. Thirdly, the marker watershed was performed to separate adherent cells and to avoid over-segmentation simultaneously. Finally, cells in phase-contrast microscopic images were counted by detecting the numbers of connected domains in the binary image. Taking the manual counting result as the counting standard and MIS, INC, and ACC are used as evaluation indicators. The experimental results showed that the average values of MIS, INC, and ACC of the proposed method are only 3.31%, 3.49%, and 96.69%, respectively. Additionally, each cell image was counted only takes 0.65 s on averagely. To further test the performance of the proposed method, a comparative experiment was carried out by Image J, and the result shows that the proposed method has a better counting performance with a higher average accuracy of 96.55% to Image J with 93.39%. The proposed method for cell counting is simple, feasible, fast and high accurate, and it can be used as an effective method for cell counting of the phase-contrast microscopic images.

## KEY WORDS

cell counting, image processing, Otsu, phase-contrast microscopic image, watershed segmentation

## 1 | INTRODUCTION

Cell counting is of great significance in biomedicine; diagnosis and treatment of most diseases require the quantitative analysis of specific cells (Chourasiya & Rani, 2014; Drey, Gruber, & Bieschke, 2013; Vayrynen et al., 2012). For example, the normal range of white blood cells (WBC) is 4,500–11,500  $\mu\text{l}^{-1}$  (Fritsma & Rodak, 2012). When the

WBC concentration is higher than 11,500  $\mu\text{l}^{-1}$ , which is commonly caused by bacteria infection instead of viral infection; when lower than 4,500  $\mu\text{l}^{-1}$ , driven mainly by medical intervention like antibiotics use with long-term and chemotherapy in cancer. WBC counting provides a high diagnosis value in acute infections and chronic disease treatment (Lorenzo & CeciliaDi, 2013; Wang, Lin, Cui, Zhou, & Liu, 2017). Analogously, cancer is closely related to the number of

immune cells in the human body (Hanahan & Weinberg, 2000). According to the number change of immune cells in the diseased tissue, the stage of cancer can be accurately determined. In the study of the antitoxic drugs which inoculated on virus-infected cells, whether the selected drug is lethal to the virus can be determined by counting the number of living cells and infected cells; in this way, the effective treatment drugs can be finally screened. And the cell counting researches also contribute to different tumor types (Coates et al., 2015), understand the cellular and molecular genetic mechanisms (Solnica-Krezel, 2005), and provide helpful information to many other applications (Forero, Kato, & Hidalgo, 2012; He, Minn, Solnica-Krezel, Anastasioe, & Lie, 2021; Vayrynen et al., 2012).

Recombinant adeno-associated virus (rAAV) is characterized by its high safety, low immunogenicity, broad host range, and the ability to mediate long-term stable expression of genes in animals. Therefore, it is regarded as one of the most promising gene therapy carriers (Flotte, 2004; Mingozi & High, 2011). However, the transduction efficiency of rAAV is relatively limited; how to improve the transduction efficiency of rAAV has been one of the hot research fields of gene therapy (Kondratov, Marsic, Mietzsch, Heilbronn, & Zolotukhin, 2016; Wang et al., 2014b; Wang et al., 2016). In our research, rAAVs of different serotypes were used to infect Hela cells. Then microscopic images of Hela cells were collected by IncuCyte ZOOM to study the transduction efficiency of the rAAV. However, the adherent cells in microscopic images were identified as only one cell by the support software of IncuCyte ZOOM during Hela cell counting. And the more significant the cell density, the worse the recognition effect, which eventually leads to considerable counting errors. Figure 1 shows the cell counting results of IncuCyte ZOOM. Besides, the Hela cell is a vital tool in medical research, and it has been widely used in cancer researches, biological or cell culture experiments. Consequently, this paper aims to study the Hela cells counting for the microscopic images under the phase contrast modality. Hela cell counting needs to be addressed urgently to enable rAAV transduction efficiency research and other studies based on Hela cells.

Traditionally, manual counting under a microscope is time-consuming and inefficient, requires a lot of workforce and expertise, and is subject to the observer's subjectivity during the cell counting process. The combinations of these factors further lead to counting errors (Zimmermann, Ruprecht, Kainzinger, Heppner, & Weimann, 2011). Although there are hardware instruments such as the Flow Cytometry and Automated Hematology Counter to perform counting, most of these devices are so expensive that many laboratories cannot afford to deploy them. The most important is that the

spatial position will be destroyed if the cell samples are moved to these instruments for counting. Yet, the spatial position information of the sample is of great significance for some researches of cells. Various cell counting methods based on microscopic images have been widely proposed in the past references, there are still many challenges for counting, as shown in Figure 2. Firstly, cells have various shapes. Secondly, cells have tiny and slender structures, which may lead to over-segmentation. Thirdly, cells tend to adhere to each other or even form clusters due to cell interaction, and the cell contour becomes blurred. Finally, microscopic images are usually low in contrast and contain many background impurities, such as cell debris and other particles (Yi et al., 2019). These problems have caused many difficulties for cell counting. Given the above issues, the automatic counting method with simple, fast, low-cost and high accuracy properties for microscopic images is highly demanded.

This article is structured as follows. The Section 2 describes related research works in cell counting. The Section 3 describes the sources of cell microscopy image data used in the approach. The Section 4 describes the specific process of the proposed method for cell counting, which is mainly divided into three parts: image preprocessing, cell segmentation, and cell counting. The Section 5 shows the results of the proposed method and manual counting. The Section 6 introduces evaluation indicators and some discussions of our proposed method. Finally, the conclusion is summarized in the Section 7.

## 2 | RELATED WORKS

Various image processing methods have been applied to cell detection and cell counting during past decades, as digital microscopes and other imaging technologies are widely used in biological experiments and clinical applications. For example, Li, Zhou, Liu, Wang, and Guo (2015) proposed a method that combines active contour models and automated two-dimensional k-means with a spectral angle mapper algorithm to segmentation and counted red blood cells. Sui and Wang (2013) proposed using a sliding band-pass filter to enhance the image to count high-density cells. This counting method has high accuracy and strong reliability; however, it measures inefficiency and takes about 15 min for cell detection of each  $775 \times 917$  image. Grishagin (2015) converted RGB images into grayscale images for binary image segmentation based on the grayscale threshold algorithm, and cell image counting was implemented by calculating black particles of a specific shape and size. This approach takes 2–10 times

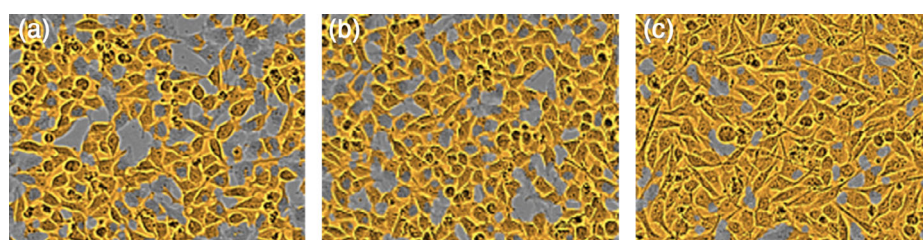


**FIGURE 1** Cell counting results by the support software of IncuCyte ZOOM. (a–c) are the counting effects with different cell densities by IncuCyte ZOOM. Adherent cells were identified as one cell, and the denser cells, the greater the counting error



**FIGURE 2** Illustration of counting challenges in cell micrograph. Cells often have variant shapes, slender structures and obscure contours, and the cells adhere or overlap each other. Microscopic images of cells are usually blurred and low in contrast, contain many background impurities and exist a lot of noise. Different images have different cell densities, and the higher the cell density, the more difficulties for counting

less time than manual counting. However, the method based on threshold segmentation is prone to over-segmentation when the cell density in the image is large. Therefore, the counting accuracy and versatility of this approach still need to be improved. Choudhry proposed an automated colony and cell counting method based on edge detection of a digital image (Choudhry, 2016), and this method is automatic, fast and very suitable for high-throughput screening. However, since edge detection operates by detecting changes of grayscale values, it fails to count for the low resolution or unfocused images. It is susceptible to miscounting the merged cell colonies.

At present, there are many commercial software tools and free software that can be used for cell detection and segmentation, such as Image J (Drury et al., 2011), cell-profiler (Usaj, Torkar, Kanduser, & Miklavcic, 2011), OpenCFU (Geissmann, 2013), cell c, image-pro, and IncuCyte ZOOM. However, people can only use these tools to process microscopic images of specific cell types and low cell density (Byun, Verardo, Sumengen, Lewis, & Fisher, 2006; Sui & Wang, 2013). Moreover, cell images collected from different fields of microscope and periods cannot be counted in batches due to the significant difference in cell densities and image resolutions and the need for parameters adjustment continuously for counting. In recent years, with the development of machine learning and deep neural network technology and their remarkable effects in target detection, deep learning applications to cell counting have received more attention. To name a few, Yi et al. (2019) proposed an attentive cell instance segmentation model, which combines a single-point multibox detector (SSD) with a U-Network on a joint network, and the attention mechanism was adopted in both detection and segmentation modules to capture nerve cell instances and accurately quickly. Song, Sanchez, ElDaly, and Rajpoot (2019) proposed a Syn-AHDA (synchronized asymmetric hybrid deep autoencoder) network for cell detection and classification simultaneously, and a neighborhood selection mechanism was adopted to improve detection and classification accuracy. This

method attained better detection and classification performance with a shorter training time compared to other deep learning frameworks. Alahmari proposed a deep learning-based unbiased stereology approach to automatically segment and estimate the total number of immunostained neurons on tissue sections (Alahmari et al., 2019). Compared to the manual stereology, the deep learning method realized over five times greater counting efficiency and less than 2% error of the counting results, which avoid subjectivity, recognition bias, and poor precision. Liu et al. proposed a counting method based on deep learning, which extracted both dot density map and foreground mask of the cell image, and then two high-level image features were stacked together with the two-input deep convolutional neural network (DCNN) model to regress to the cell counts (Liu, Junker, Murakami, & Hu, 2019). By assembling deep imaging features with DCNN, this method improved cell counting and has a better counting performance of microscopic images. In summary, cell detection and segmentation research based on deep learning is currently optimal, while deep learning models require a large amount of training data to show magical effects. Counting methods based on deep learning cannot be performed when the micrograph samples are too small.

To overcome the deficiencies mentioned above and make cell counting simple, efficient and low-cost, an automatic counting method based on the combination of Otsu and marker-controlled watershed segmentation for Hela cell microscopic images was proposed in this paper. Otsu method was used to obtain the optimal threshold of image binarization to segment cells preliminarily. The marker watershed was used to further segment adherent cells to avoid over-segmentation and improve counting accuracy. Finally, cell counting was realized by detecting the connected domains in binary images (Zhu, Wang, Liu, & Mi, 2018), which dramatically reduces the subjective influence of laboratory personnel. The proposed method for cell counting is fast, has high accuracy and efficiency, robust reliability, and low cost, and is of great significance to the fundamental researches of biomedicine. This article makes following several contributions:

1. An automatic fast counting method for dense Hela cells designed explicitly for phase contrast microscopy is proposed.
2. The method of stepwise segmentation using Otsu and watersheds solves the problem of connection interference in cell segmentation and improves the segmentation effect.
3. Established a cell counting sample library of phase-contrast micrographs of Hela cells.
4. Realize batch counting, cropping and saving of cell images.

### 3 | MATERIALS AND METHODS

Microscopic images of cells were collected from experiments that AAVs of different serotypes infected Hela cells. Image acquisition was performed with the IncuCyte Zoom imaging system, which supports high-resolution phase contrast. The objective lens specification is Nikon 10×, and the size of each image is 1,392 × 1,040 and saved in

TIF format. There are 128 cell images collected in our experiment. The microscopic images acquired by the IncuCyte ZOOM imaging system by default are large, and the number and the density of cells in the image are large (4,000–5,000 cells per image), which is not conducive to the observation of the cell counting effect and the analysis of the accuracy rate in the later period. Therefore, the collected 128 microscopic images of cells were cropped in batches by MATLAB R2017b. Each image was divided into 16 pictures of the same size and saved in TIF format. Finally, we collected 2048 cell images for the counting research. The size of each image was  $348 \times 260$ , and the microscopic image data set of Hela cells for counting research is shown in Figure 3.

## 4 | METHODOLOGY

The overall process of microscopic image cell counting is mainly divided into three parts: image preprocessing, cell segmentation, and cell counting, as shown in Figure 4. This experiment uses the MATLAB R2017b image processing toolbox to process the collected cell microscopic images. Firstly, the contrast of an image is enhanced, and the median filter eliminates the noises during image preprocessing. Then the Otsu method is used to obtain the optimal threshold to binarize the microscopic image so that the cells are segmented from the background. Next, the adhered cells were separated by the watershed segmentation algorithm. Finally, cell counting was achieved by counting the number of connected domains in the microscopic image.

### 4.1 | Image preprocessing

#### 4.1.1 | Image contrast enhancement

Due to the factors such as light, interference of various parameters, and limitations of the performance of the receiving device, the contrast between the cells and the background in the acquired

microscopic images is usually insufficient, and the cell outline is blurred, which brings challenges to the further counting works. In this article, the contrast linear widening (Kim, Kim, Jung, Noh, & Ko, 2011; Yang, 2006) is used to suppress the gray value of the interstitial space in the microscopic image to solve these problems. The gray values of the cells in the original image are re-mapped to enhance the cell outline. Figure 5a shows the original cell image, and the image of enhanced cell contrast is shown in Figure 5b. Then the grayscale value 120 is set as the threshold to enhance the cell image further. The result of image contrast enhancement with a threshold is shown in Figure 5c, which makes the cell outline and its distribution more apparent, and the image is more advantageous for observing.

#### 4.1.2 | Median filter

Image filter is to eliminate image noises under the condition of preserving image details as much as possible. The median filter replaces the value of a point in a digital image with the median value of each point in the neighborhood, making the gray value of surrounding pixels close to the point value, which can overcome the blur problem of image details processed by a linear filter and effectively eliminate isolated noises (Chervyakov, Lyakhov, & Orazaev, 2018; Lin, 2007). In this paper, a median filter with the neighborhood size of  $3 \times 3$  was applied to the image preprocessing step for eliminating noises. The image after the median filter is shown in Figure 5d. The noises in the cell microscopic image are effectively removed, and the median filter can better protect the edges of the image and retain the image details when filtering the noises.

### 4.2 | Cell segmentation

Image segmentation divides the image scene into two regions of interest and background, thereby simplifying or changing the image

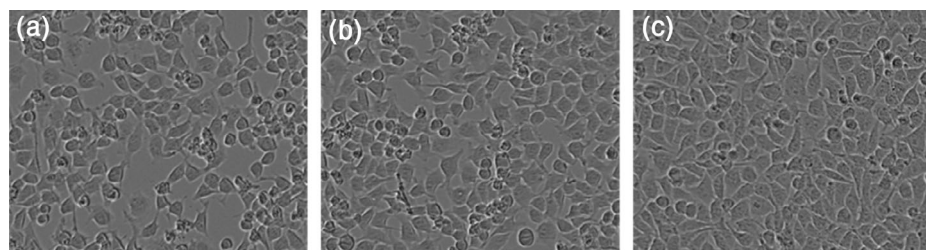


**FIGURE 3** Some sample Hela cell images of the phase-contrast microscopic image dataset. (a–c) show Hela cell microscopic images with different densities and resolutions, in which cell density increased and the image resolution decreased gradually

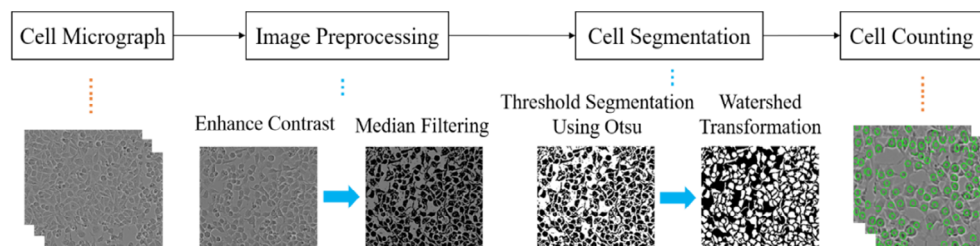


**FIGURE 4** Overall flowchart of the automatic counting method for Hela cell images based on the combination of Otsu and marker-controlled watershed segmentation

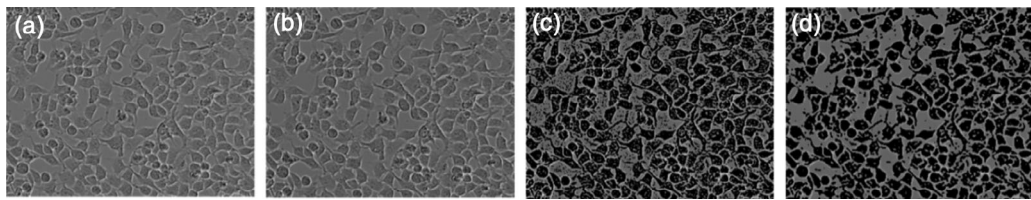


**FIGURE 5** Results of cell image preprocessing. (a) Original cell image. (b) Enhancement Images after contrast enhance. (c) Image enhancement with the threshold, the cell outline and the detailed information of the image become clearer. (d) Cell median filtered image, the discrete noise is effectively removed, and the edge detail information of the cell image can be better protected

representation and making image analysis easier (Al-Kofahi, Lassoued, Lee, & Roysam, 2010; Meijering, 2012; Sharma & Aggarwal, 2010). As shown in Figures 2 and 3 above, cell profiles are blurred. The contrast, cell density, and cell resolution of different microscopic images significantly differ, which brings significant challenges to cell counting. Image segmentation processing should be performed based on an adaptive global threshold to realize batch counting of cell images. Besides, the cell adhesion and overlap may lead to significant counting errors.

Otsu method is characterized by its simple procedure, nonparametric and unsupervised nature of threshold selection (Otsu, 2007; Xu, Xu, Jin, & Song, 1998), which can automatically and stably select an optimal global threshold for image segmentation. The watershed algorithm can effectively segment its adherent objects. Therefore, the Otsu method was applied to automatically select the optimal global binarization threshold for initial segmentation in this paper. Then, the adherent cells were further segmented based on the marker watershed to reduce counting errors. The application of the Otsu method and watershed algorithm ensures the batch counting of cell images and the accuracy of counting results.

#### 4.2.1 | Binarization of cell image based on Otsu method

Otsu was performed to obtain the optimal threshold automatically for image binarization, and the specific procedure is shown as follows. Assume that the given microscopic image of the cell is represented as  $K$  gray level ( $1, 2, \dots, K$ ),  $i$  denotes the gray level,  $n_i$  denotes the number of pixels at  $i$  gray level,  $N$  denotes the total number of pixels, and  $P_i$  represents the probability of occurrence of level  $i$  (Cheriet, Said, & Suen, 1998; Otsu, 2007; Xu et al., 1998).

$$P_i = n_i/N, \quad (1)$$

The given microscopic images of the cell were divided into two classes by threshold  $t$ , cells and background, which are consisted of gray level  $[1, \dots, t]$  and  $[t + 1, \dots, K]$  respectively, and the optimal threshold for cell segmentation is obtained when the value of between-class variance is the Maximum (Xu et al., 1998). The between-class variance  $\sigma^2$  and optimal threshold  $T$  are given by

$$\sigma^2 = \chi_0(\varphi_0 - \varphi)^2 - \chi_1(\varphi_1 - \varphi)^2 = \chi_0\chi_1(\varphi_0 - \varphi_1)^2, \quad (2)$$

$$T = \underset{1 \leq t \leq K}{\operatorname{Max}} \{\sigma^2\}, \quad (3)$$

where,  $\chi_0$  and  $\chi_1$  denote the possibility of the occurrence of cells and background,  $\varphi_0$  and  $\varphi_1$  denote the mean level of the cells and background, and  $\varphi$  is the mean level of the image, defined as follows

$$\varphi = \sum_{i=1}^K i P_i = \chi_0 \varphi_0 + \chi_1 \varphi_1, \quad (4)$$

The microscopic cell images were binarized by the optimal threshold  $T$ , as the Equation (5) shown, which simplifies the image and achieves the excellent segmentation performance of the target cells.

$$G(x,y) = \begin{cases} 0, & g(x,y) \leq T \\ 1, & g(x,y) > T \end{cases} \quad (5)$$

At the same time, the cell profiles are highlighted, which provides good working conditions for subsequent cell counting. The binarized cell image is shown in Figure 6a. Then color inversion and hole filling process were performed on the image. And the result of cell image color inversion and cell hole filling is shown respectively in Figure 6b,c.

#### 4.2.2 | Adhering cells segmentation based on marker watershed

The watershed segmentation (Vincent & Soille, 1991) method is an algorithm for segmenting the target and background by simulating the flooding process of basin topography in geography. It has the advantages of simple operation, accurate positioning and obtainable continuous closed segmentation edge and has attracted the attention of many scholars and experts. However, the traditional watershed algorithm is prone to over-segmentation during image processing, which seriously interferes with extracting real targets. The over-segmentation can be reduced by controlling the markers. Therefore, in this paper, the maker watershed algorithm was adopted to segment the adherent cells to improve cell counting accuracy (Gao, Yang, &

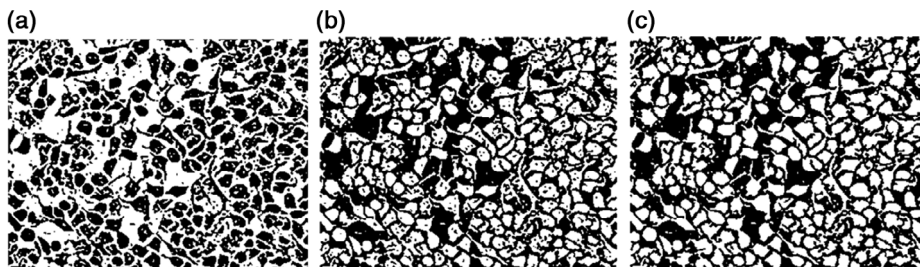


**FIGURE 6** (a) The binary result by Otsu method. (b) Cell image color inversion. (c) Image of cell hole filling



**FIGURE 7** Illustration of the segmentation results based on the marker-controlled watershed. (a) The whole image result after watershed segmentation. (b) Images before watershed segmentation, some cell structures adhere to each other. (c) Results of watershed segmentation. Adherent cells were separated and will not be regarded as only one cell

Li, 2007; Wang, 2017; Wang, Dong, & Wang, 2014a). The specific process of marker watershed segmentation is as follows.

#### Construct distance topographic map and extract the cell markers

The distance topographic map can be regarded as a topological surface corresponding to the topographic surface of the basin. And the local minima in the distance map correspond to the core of cells, that is, the target location, which is called a marker (Miao, Liang, Liu, & Ding, 2016). Euclidean distance transformation was performed on the image of cell hole filling ( $G_1$ ) to obtain the distance map. The formula of distance transformation is given

$$G_2 = \text{bwdist}(x_0, y_0) = \sqrt{(x_0 - x_n)^2 + (y_0 - y_n)^2}, \quad (6)$$

where,  $\text{bwdist}(\cdot)$  represents the distance transformation between minimum area pixels and boundary pixels;  $G_2$  represents the distance map.

#### Eliminate local minima

Ideally, a marker corresponds to a target location (cell), but there are often many pseudo-local minimum points in the distance map. It will lead to over-segmentation if the number of markers exceeds the number of target cells. Therefore, the extended minimum technology (H-minima transform [Yu, Hou, & Song, 2011]) was applied to eliminate the local minima, which were smaller than  $h$ , to obtain the markers image. The specific process is expressed by the following formula:

$$G_3 = \text{imextendedmin}(G_2, h), \quad (7)$$

where,  $G_3$  represents the markers image,  $\text{imextendedmin}(\cdot)$  represents the H-minima transform, and  $h$  is the manual threshold for H-minima transform operation.

#### Modify the distance map

After obtaining the markers image, the original local minima value in the distance topographic map  $G_2$  were replaced by the cell markers image  $G_3$ , so that the local minima value in the distance map only exist at the positions of the markers, that is, each marker corresponds to a cell, thereby suppressing the over-segmentation.

$$G_4 = \text{imposemin}(G_2, G_3), \quad (8)$$

where,  $\text{imposemin}(\cdot)$  means mandatory minima calibration operation, finally, the watershed transform was performed on the image  $G_4$  to obtain the segmentation result of the adhesion cells, which is denoted as  $I_{ws}$ . And the specific results of the adherent cells segmentation based on the marker watershed are shown in Figure 7.

$$I_{ws} = \text{watershed}(G_4), \quad (9)$$

### 4.3 | Cell counting

A series of images processing preprocess the cell microscopic image to form a binarized image. The binaries image's cell pixels are labeled as 255, and the background is labeled as 0. To calculate the number of cells, the binary image is converted into a matrix consisting of only

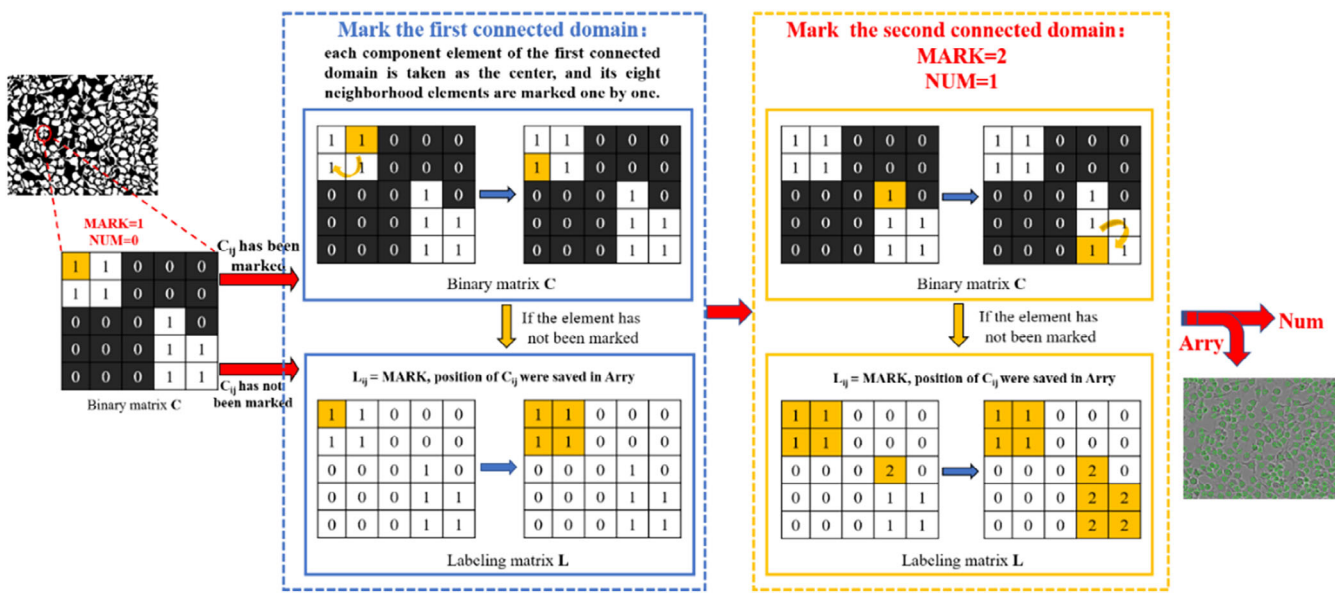


**FIGURE 8** Illustration of the cell counting process. One connected domain, which is consisted of element value 1 in matrix C, represents a single cell. Scan C matrix, if the value of element 1 is encountered, it will be marked in labeling matrix L. The element's coordinate is saved in Arry, and a green counting circle is drawn on the original image according to the coordinates in Arry until all elements of the first connected domain are marked. Similarly, mark other connected domains in C, and the numbers of connected domains are finally returned with NUM until all connected domains are labeled, namely total the cell numbers

0 and 1. That is, the cell pixels in the binary image are represented by 1, and the background pixels in the binary image are represented by 0. The calculation formula is:

The cell pixels in the binarized image are labeled as 1, the background is labeled as 0, and every connected domain in the binary image represents a single cell. Consequently, traversing matrix (C) corresponds to the binary image and returns the final connected domain number (NUM) to realize automatic and fast counting of cells. Figure 8 illustrates the cell counting process, and the specific steps are as follows:

- Firstly, the connected domain label variable (MARK) is initialized 1, and the connected domain total variable (NUM) is initialized to 0.
- It starts from the first row and the first column in matrix C, traversing the elements in the matrix from left to right and from top to bottom. When the element  $C_{ij}$  with a value of 1 in the matrix is detected, determine whether MARK has marked the element. If the element is already marked, the other eight neighborhood (up, down, left, right, upper left, upper right, lower left, and lower right) elements of the  $C_{ij}$  are scanned; If it is not marked, the value of MARK is assigned to the element  $L_{ij}$  at the corresponding position in labeling matrix L for labeling, and save the value of the pixel corresponding to the element  $L_{ij}$  to the queue (Array).
- Then take the element  $C_{ij}$  as the center and continue to traverse the elements of its eight neighborhoods. When an element with a value of 1 in the eight neighborhoods is detected, determine whether the element is labeled. If it is no label, use MARK to label

in the L, and the value of the pixel corresponding to the element is stored in Arry.

- After the matrix element,  $C_{ij}$  and its eight neighborhoods are scanned and labeled, the next element  $C_{ij+1}$  and its eight neighborhoods are scanned and labeled;
- When a connected domain completes marking, both the value of NUM and MARK are incremented by one, the Arry is cleared, and a new connected domain is to be marked;
- Loop through the entire binary image matrix until the labeling of all connected domains is completed, and the total number of connected domains (NUM) returned is the number of cells in the binary image.

During the process of labeling connected domains, the coordinate values of pixels of the connected domain are stored in the Arry. By identifying different connected domains in the labeling matrix, the horizontal and vertical coordinate values of the pixels constituting each connected domain are returned to the r and c matrices, respectively, then calculate the average values of the horizontal and vertical coordinates of the connected domain (rbar and cbar). Finally, rbar and cbar were considered as the center of the circle, and green circles were drawn on the original cell microscopic image as the counting marker of the cell.

## 5 | EXPERIMENTAL RESULTS

Two thousand and forty eight Hela cell microscopic images with  $348 \times 260$  were counted and saved in batches, and several images of

counting results are shown in Figure 9. Among them, 28 images were randomly selected as sample images to analyze the experimental, and the counting results of proposed methods (PCN) of these images are shown in Table 1.

The 28 cell images were counted manually again to evaluate the counting performance of the proposed method. Taking the original image as the counting standard, and based on the counted images of the proposed method, visually identify whether there are indeed cells

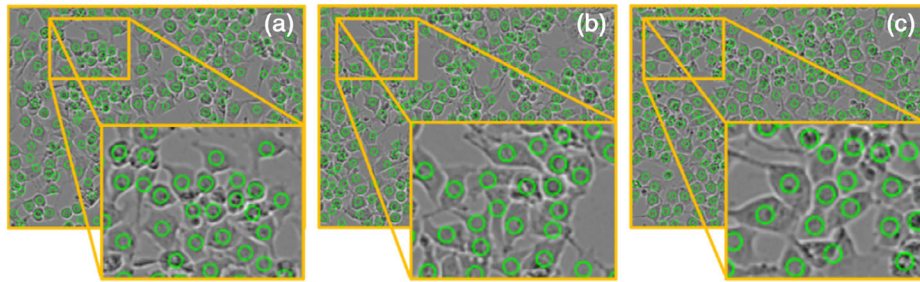
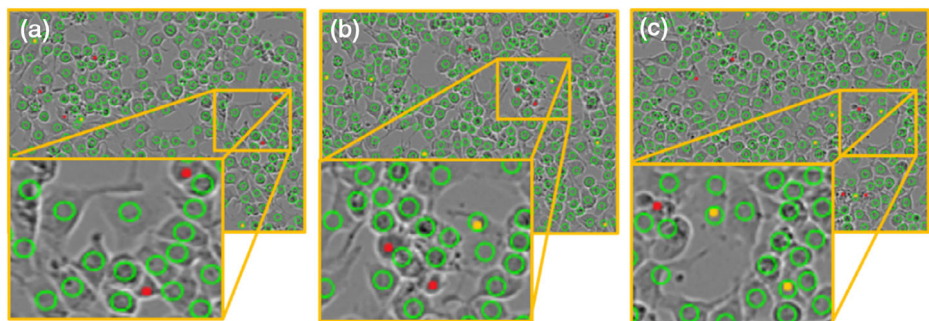


**FIGURE 9** The part figures (a–c) show the part cell counting results of the proposed method

Cell images	MCN	Evaluation (%)						
		PCN	MN	IN	MIS	INC	ACC	Time(s)
Image 1	309	308	9	8	2.92%	2.59%	97.09%	1.66
Image 2	310	303	10	3	3.30%	0.97%	96.77%	0.67
Image 3	293	296	9	12	3.04%	4.10%	96.93%	0.67
Image 4	302	297	14	9	4.71%	2.98%	95.36%	0.62
Image 5	273	270	15	12	5.56%	4.40%	94.51%	0.74
Image 6	292	285	13	6	4.56%	2.05%	95.55%	0.57
Image 7	289	289	6	6	2.08%	2.08%	97.92%	0.55
Image 8	287	284	10	7	3.52%	2.44%	96.52%	0.64
Image 9	286	287	9	10	3.14%	3.50%	96.85%	0.56
Image 10	312	310	11	9	3.55%	2.88%	96.47%	0.58
Image 11	302	302	11	11	3.64%	3.64%	96.36%	0.61
Image 12	285	289	9	13	3.11%	4.56%	96.84%	0.65
Image 13	305	307	7	9	2.28%	2.95%	97.70%	0.57
Image 14	311	314	7	10	2.23%	3.22%	97.75%	0.60
Image 15	272	275	6	9	2.18%	3.31%	97.79%	0.58
Image 16	285	276	17	8	6.16%	2.81%	94.04%	0.61
Image 17	286	289	14	17	4.84%	5.94%	95.10%	0.61
Image 18	277	281	11	15	3.91%	5.42%	96.03%	0.65
Image 19	256	266	7	17	2.63%	6.64%	97.27%	0.62
Image 20	305	304	9	8	2.96%	2.62%	97.05%	0.65
Image 21	323	327	7	11	2.14%	3.41%	97.83%	0.58
Image 22	307	314	14	21	4.46%	6.84%	95.44%	0.55
Image 23	316	322	6	12	1.86%	3.80%	98.10%	0.60
Image 24	296	305	9	18	2.95%	6.08%	96.96%	0.57
Image 25	312	313	8	9	2.56%	2.88%	97.44%	0.67
Image 26	343	341	10	8	2.93%	2.33%	97.08%	0.63
Image 27	337	337	6	6	1.78%	1.78%	98.22%	0.59
Image 28	303	297	11	5	3.70%	1.65%	96.37%	0.60
Average	299	300	10	10	3.31%	3.49%	96.69%	0.65

**TABLE 1** Analysis of cell microscopic image counting experiment data

**FIGURE 10** The part figures (a–c) show the part results of manual cell count. The red dots in the figure indicate missed count cells, and the yellow dots indicate incorrect counted cells



in the corresponding position of the green circle on the image or whether there are repeated green circles on the same cell. And the red dots were used to mark the missed count cells, and the yellow dots were used to mark incorrect count cells. Several results of the manual cell counting are shown in Figure 10, and the numbers of manual cell counting (MCN), missed count cells (MN), and incorrect count cells (IN) are shown in Table 1. As shown in Figure 11, PCN is very close to MCN, and the fluctuation range is only 0–9 cells. Compared to the total cell count, both MN and IN are small, which could be accepted. Accordingly, the counting results of the proposed method are reliable in terms of the cell count value.

We take the results of manual cell counting as the standard, and three evaluation indicators further analyzed the counting effect of the proposed method: accuracy (ACC), missed count rate (MIS), and incorrect count rate (INC). The definitions of MIS, INC and ACC are given:

$$MCN = PCN + MN - IN, \quad (10)$$

$$MIS = \frac{MN}{PCN} \times 100\%, \quad (11)$$

$$INC = \frac{IN}{MCN} \times 100\%, \quad (12)$$

$$ACC = \frac{PCN - IN}{MCN} \times 100\%, \quad (13)$$

where, MCN is the number of manual cell count, PCN is the cell count number of the proposed method; MN is the number of missed count cells, and IN is the number of incorrect count cells.

As shown in Figure 12, the average ACC of the proposed method is as high as 96.69%, and the ACC range is 94.04–98.22%; The average MIS is 3.31%, and the MIS range is 1.78–6.16%; The average INC is 3.49%, and the INC ranges from 0.97% to 6.64%. The whole process from acquiring one cell image to save the counting result was completed within 1.7 s, and each cell image with the size of  $348 \times 260$  is counted only takes 0.65 s on average. The specific data related to the cell counting aforementioned are shown in Table 1. The experimental results show that compared with manual counting, the proposed method has higher counting accuracy, faster processing, and more efficiency for cell image counting.

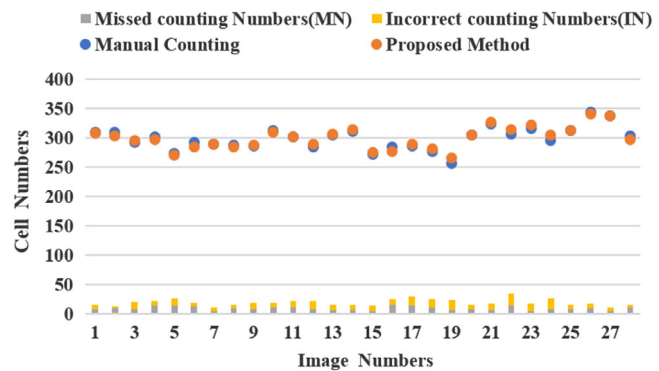


**FIGURE 11** Cell counting results compared between manual and proposed methods. The X-axis represents the image numbers in the dataset; Y-axis represents the cell numbers. As the stacked column in the figure shown, compared with the total number of cells in the image, the MN and IN of the proposed method are very small, which indicates the counting results of the proposed method are reliable

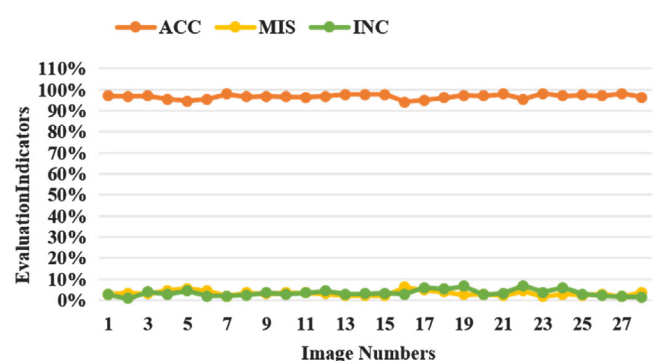


**FIGURE 12** Evaluation of the proposed method counting effect

## 6 | DISCUSSION

State of the art approaches for cell counting is mainly based on deep learning or machine learning, requiring a large amount of training data to show magical effects, and the cell annotation will be a considerable workload. Moreover, even though some deep learning or machine learning models have good test results on their own data sets, it is still difficult to ensure the robustness when they are applied to Hela cell

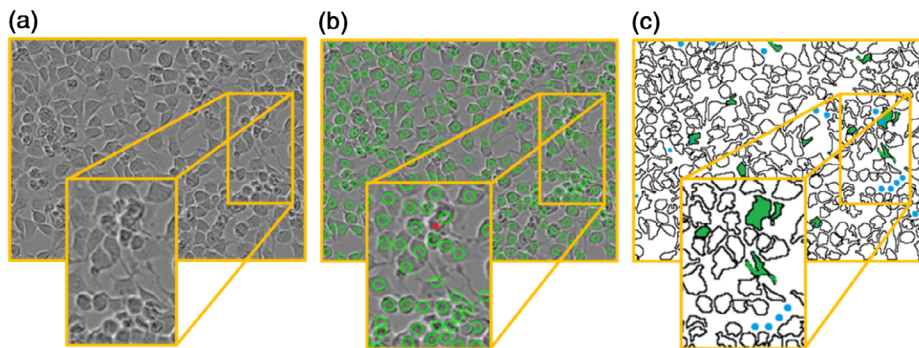


**FIGURE 13** Cell counting results compared between Image J and proposed methods. (a) Original cell image. (b) Cell counting results of the proposed method. (c) Counting results of the Image J. The contours of the cells that are incorrectly counted are filled with green, and the missed count cells are marked with blue dots

Cell images	Cell numbers (CN)			ACC		MIS		INC	
	MCN	PRO	IMJ	PRO	IMJ	PRO	IMJ	PRO	IMJ
Image 1	293	296	288	96.93%	93.17%	3.04%	6.94%	4.10%	5.12%
Image 2	302	297	297	95.36%	91.06%	4.71%	9.09%	2.98%	7.28%
Image 3	289	289	284	97.92%	93.77%	2.08%	6.34%	2.08%	4.50%
Image 4	312	310	309	96.47%	90.06%	3.55%	10.03%	2.88%	8.97%
Image 5	273	275	288	97.80%	96.34%	2.18%	2.08%	2.93%	9.16%
Image 6	285	276	284	94.04%	94.04%	6.16%	5.99%	2.81%	5.61%
Image 7	277	281	276	96.03%	92.06%	3.91%	7.61%	5.42%	7.58%
Image 8	323	327	341	97.83%	96.59%	2.14%	3.23%	3.41%	8.98%
Average	294	294	296	96.55%	93.39%	3.47%	6.41%	3.32%	7.15%

images as the shapes of normal Hela cells are far from the other normal cells. And the most important is that the proposed method in this paper focuses on the application of cell counting in the laboratory rather than the algorithms refreshing.

Image J, the counting software, is generally accepted and widely used in the field of biomedical research. To further test the counting reliability of the proposed method and make it more objective, a comparative experiment was carried out between the proposed method and Image J. And 8 out of the 28 sample images were randomly selected and then counted with Image J, and the contour of each cell in the images was kept for subsequent analysis. Taking the original cell image as the standard, the contours of the cells miscounted by Image J were filled with green and the cells missed by Image J were marked with blue dots. The counting results of Image J and the proposed method are shown in Figure 13, and the specific data are shown in Table 2.

The average counting accuracy of Image J is 93.39%, and the average accuracy of the proposed method is 96.55%. The average MIS and INC of Image J are as high as 6.41 and 7.15%, respectively, while the average MIS and INC of the proposed method are only 3.47 and 3.32%. The comparative experiments show that the cell counting accuracy of the proposed method is significantly higher than that of Image J, and MIS and INC are also far lower than Image J. The cell counting performance of the proposed method is better than that of Image J. In addition, although Image J has powerful

image processing functions due to the integration of multiple method modules, various modules selections and parameter adjustments are still required in practical applications, and the counting efficiency is relatively low. Unlike the other existing counting methods, different microscopic images need to be continuously debugged to obtain higher counting accuracy. The proposed method can process cell images automatically, realize batch reading, counting and storage, and the counting accuracy will not change significantly with the increase of image cell density, which has a relatively stable counting performance.

Because the number of cells in the whole image is too large, to analyze the counting effect, the collected image is divided into 16 pictures of the same size for counting research, resulting in the destruction of cells at the edge of the image, which will inevitably have a certain impact on the counting accuracy. However, this deviation is still acceptable in biomedical cell counting experiments. Besides, the main factors affecting cell counting are uneven illumination and noise of microscopic images. Image preprocessing and cell segmentation will be the focus of future research. Finally, although the proposed method has a good counting effect on Hela cell microscopic images and solves the problem we encountered in the study of rAAV transduction efficiency, a satisfactory cell counting method should be applicable for other types of microscopic images, so we will take the further research based on the proposed approach to make it suitable for counting other cell images.

**TABLE 2** Count comparison between Image J and the proposed method (PRO, proposed method; IMJ: Image J)

## 7 | CONCLUSIONS

In this paper, an automatic counting method for Hela cell of phase contrast microscopic images based on the combination of Otsu method and marker-controlled watershed segmentation is proposed, and it enables batch counting of Hela cell images. The performances of the proposed method were evaluated by the following three indicators: ACC, MIS, and INC. The average ACC of the proposed method for cell microscopic image counting is 96.69%. The highest ACC is 98.22%. The average MIS is 3.31%, and the average INC rate is 3.49%, which meets the cell counting requirements of the biomedical laboratory. To further test the counting effect of the proposed method, a comparative experiment is carried out with Image J, and the result shows that the proposed method has a better counting performance with the higher accuracy and average MIS and the lower average MIS.

The proposed method combined with digital image processing technology greatly improves the cell counting efficiency and reduces the labor intensity of researchers. On the other hand, it also dramatically eliminates the subjective effects of artificial cell counting, making the cell counting result more objective. It is an automatic, simple, efficient, low-cost, and reliable counting method of great significance for basic research in biomedicine.

## ACKNOWLEDGMENTS

This work was supported by Fujian Provincial Science and Technology Major Project (No.2020HZ02014)and the Promotion Program for Young and Middle-aged Teacher in Science and Technology Research of Huaqiao University (No.ZQN-PY518), and the grants from the National Natural Science Foundation of China (Grant No.61605048), in part by Fujian Provincial Big Data Research Institute of Intelligent Manufacturing, in part by the Quanzhou scientific and technological planning projects (No. 2018Z176, 2018C113R, 2019C028R, 2019C029R, 2019C076R and 2019C099R).

## CONFLICT OF INTEREST

The authors declare no conflicts of interest.

## DATA AVAILABILITY STATEMENT

The Microscopic images data of Hela cells used to support the findings of this study were supplied by the School of Medicine, Huaqiao University, Quanzhou, China, under license and can be made freely available.

## ORCID

Yuefei Lin  <https://orcid.org/0000-0002-5404-3255>

## REFERENCES

- Alahmari, S. S., Goldgof, D. B., Hall, L. O., Phoulady, H. A., Patel, R. H., ... Mouton, P. R. (2019). Automated cell counts on tissue sections by deep learning and unbiased stereology. *Journal of Chemical Neuroanatomy*, 96, 94–101.
- AI-Kofahi, Y., Lassoued, W., Lee, W., & Roysam, B. (2010). Improved automatic detection and segmentation of cell nuclei in histopathology images. *IEEE Transactions on Biomedical Engineering*, 57(4), 841–852.
- Byun, J., Verardo, M. R., Sumengen, B., Lewis, G. P., & Fisher, S. K. (2006). Automated tool for the detection of cell nuclei in digital microscopic images: Application to retinal images. *Molecular Vision*, 12, 949–960.
- Cheriet, M., Said, J. N., & Suen, C. Y. (1998). A recursive thresholding technique for image segmentation. *IEEE Transactions on Image Processing*, 7(6), 918–921.
- Chervyakov, N. I., Lyakhov, P. A., & Orazaev, A. R. (2018). New methods of adaptive median filtering of impulse noise in images. *Computer Optics*, 42(4), 667–678.
- Choudhry, P. (2016). High-throughput method for automated colony and cell counting by digital image analysis based on edge detection. *PLoS One*, 11(2), e0148469.
- Chourasiya, S., & Rani, G. U. (2014). Automatic red blood cell counting using watershed segmentation. *Hemoglobin*, 14, 17.
- Coates, A. S., Winer, E. P., Goldhirsch, A., Gelber, R. D., Gnant, M., Piccart-Gebhart, M., ... Xu, B. (2015). Tailoring therapies—Improving the management of early breast cancer: St Gallen international expert consensus on the primary therapy of early breast cancer 2015. *Annals of Oncology*, 26(8), 1533–1546.
- Drey, L. L., Gruber, M. C., & Bieschke, J. (2013). Counting unstained, confluent cells by modified bright-field microscopy. *BioTechniques*, 55(1), 28–33.
- Drury, J., Nik, H., Van Oppenraaij, R. H. F., Tang, A., Turner, M. A., ... Quenby, S. (2011). Endometrial cell counts in recurrent miscarriage: A comparison of counting methods. *Histopathology*, 59(6), 1156–1162.
- Flotte, T. R. (2004). Gene therapy Progress and prospects: Recombinant adeno-associated virus (rAAV) vectors. *Gene Therapy*, 11(10), 805–810.
- Forero, M. G., Kato, K., & Hidalgo, A. (2012). Automatic cell counting *in vivo* in the larval nervous system of drosophila. *Journal of Microscopy*, 246(2), 202–212.
- Fritsma, G. A., & Rodak, K. (2012). *Hematology: Clinical principles and applications*. St. Louis, MI: Elsevier Saunders.
- Gao, L., Yang, S. Y., & Li, H. Q. (2007). New unsupervised image segmentation via marker-based watershed. *Journal of Image and Graphics*, 12(6), 1025–1032.
- Geissmann, Q. (2013). OpenCFU, a new free and open-source software to count cell colonies and other circular objects. *PLoS One*, 8(2), e54072.
- Grishagin, I. V. (2015). Automatic cell counting with ImageJ. *Analytical Biochemistry*, 473, 63–65.
- Hanahan, D., & Weinberg, R. A. (2000). The hallmarks of cancer. *Cell*, 100(1), 57–70.
- He, S., Minn, K. T., Solnica-Krezel, L., Anastasioe, M. A., & Lie, H. (2021). Deeply supervised density regression for automatic cell counting in microscopy. *Medical Image Analysis*, 68, 101892.
- Kim, J. H., Kim, J. H., Jung, S., Noh, C. K., & Ko, S. (2011). Novel contrast enhancement scheme for infrared image using detail-preserving stretching. *Optical Engineering*, 50(7), 077002.
- Kondratov, O., Marsic, D., Mietzsch, M., Heilbronn, R., & Zolotukhin, S. (2016). Fine tuning of transduction efficiency of rAAV vectors via modulation of capsid composition. *Molecular Therapy*, 24, S220.
- Li, Q., Zhou, M., Liu, H., Wang, Y., & Guo, F. (2015). Red blood cell count automation using microscopic hyperspectral imaging technology. *Applied Spectroscopy*, 69(12), 1372–1380.
- Lin, T. C. (2007). A new adaptive center weighted median filter for suppressing impulsive noise in images. *Information Sciences*, 177(4), 1073–1087.
- Liu, Q., Junker, A., Murakami, K., & Hu, P. (2019). Automated counting of cancer cells by ensembling deep features. *Cell*, 8(9), 1019.
- Lorenzo, P., & CeciliaDi, R. (2013). In A. Petrosino (Ed.), *Investigation of different classification models to determine the presence of leukemia in peripheral blood image* (pp. 612–621). Springer Berlin Heidelberg: Berlin, Heidelberg.

- Meijering, E. (2012). Cell segmentation: 50 years down the road [life sciences]. *IEEE Signal Processing Magazine*, 29(5), 140–145.
- Miao, H., Liang, G., Liu, R., & Ding, J. (2016). Watershed algorithm using edge gradient combined with distance transformation for segmentation of blood cells. *Journal of Image and Graphics*, 21(2), 192–198.
- Mingozzi, F., & High, K. A. (2011). Therapeutic in vivo gene transfer for genetic disease using AAV: Progress and challenges. *Nature Reviews Genetics*, 12(5), 341–355.
- Otsu, N. (2007). A threshold selection method from gray-level histograms. *IEEE Transactions on Systems, Man, and Cybernetics*, 9(1), 62–66.
- Sharma, N., & Aggarwal, L. M. (2010). Automated medical image segmentation techniques. *Journal of Medical Physics*, 35(1), 3.
- Solnica-Krezel, L. (2005). Conserved patterns of cell movements during vertebrate gastrulation. *Current Biology*, 15(6), R213–R228.
- Song, T. H., Sanchez, V., ElDaly, H., & Rajpoot, N. M. (2019). Simultaneous cell detection and classification in bone marrow histology images. *IEEE Journal of Biomedical and Health Informatics*, 23(4), 1469–1476.
- Sui, D., & Wang, K. (2013). A counting method for density packed cells based on sliding band filter image enhancement. *Journal of Microscopy*, 250(1), 42–49.
- Usaj, M., Torkar, D., Kanduser, M., & Miklavcic, D. (2011). Cell counting tool parameters optimization approach for electroporation efficiency determination of attached cells in phase contrast images. *Journal of Microscopy*, 241(3), 303–314.
- Vayrynen, J. P., Vornanen, J., Sajanti, S., Bohm, J., Tuomisto, A., ... Makinen, M. J. (2012). An improved image analysis method for cell counting lends credibility to the prognostic significance of T cells in colorectal cancer. *Virchows Archiv*, 460(5), 455–465.
- Vincent, L., & Soille, P. (1991). Watersheds in digital spaces: An efficient algorithm based on immersion simulations. *IEEE Transactions on Pattern Analysis and Machine Intelligence*, 13(6), 583–598.
- Wang, A. L., Dong, B. T., & Wang, Z. S. (2014a). Pedestrian detection of integrating BS based on quadratic reconstruction and IE marker watershed. *Journal of Transportation Systems Engineering and Information Technology*, 14(4), 72066–72112.
- Wang, Q., Dong, B., Firrman, J., Roberts, S., Moore, A. R., Cao, W., ... Xiao, W. (2014b). Efficient production of dual recombinant adeno-associated viral vectors for factor VIII delivery. *Human Gene Therapy Methods*, 25(4), 261–268.
- Wang, Q., Firrman, J., Wu, Z., Pokiniewski, K. A., Valencia, C. A., Wang, H., ... Wunder, S. L. (2016). High-density recombinant adeno-associated viral particles are competent vectors for in vivo transduction. *Human Gene Therapy*, 27(12), 971–981.
- Wang, X., Lin, G., Cui, G., Zhou, X., & Liu, G. L. (2017). White blood cell counting on smartphone paper electrochemical sensor. *Biosensors and Bioelectronics*, 90, 549–557.
- Wang, Y. (2017). Adaptive marked watershed segmentation algorithm for red blood cell images. *Journal of Image and Graphics*, 12, 1779–1787.
- Xu, X., Xu, S., Jin, L., & Song, E. (1998). Characteristic analysis of Otsu threshold and its applications. *Pattern Recognition Letters*, 32(7), 956–961.
- Yang, C. (2006). Image enhancement by modified contrast-stretching manipulation. *Optics and Laser Technology*, 38(3), 196–201.
- Yi, J., Wu, P., Jiang, M., Huang, Q., Hoeppner, D. J., ... Metaxas, D. N. (2019). Attentive neural cell instance segmentation. *Medical Image Analysis*, 55, 228–240.
- Yu, W. S., Hou, Z. Q., & Song, J. J. (2011). Color image segmentation based on marked-watershed and region-merger. *Acta Electronica Sinica*, 39(5), 1007–1012.
- Zhu, C., Wang, J., Liu, H., & Mi, H. (2018). Insect identification and counting in stored grain: Image processing approach and application embedded in smartphones. *Mobile Information Systems*, 3, 1–5.
- Zimmermann, M., Ruprecht, K., Kainzinger, F., Heppner, F. L., & Weimann, A. (2011). Automated vs. manual cerebrospinal fluid cell counts: A work and cost analysis comparing the Sysmex XE-5000 and the Fuchs-Rosenthal manual counting chamber. *International Journal of Laboratory Hematology*, 33(6), 629–637.

**How to cite this article:** Lin, Y., Diao, Y., Du, Y., Zhang, J., Li, L., & Liu, P. (2021). Automatic cell counting for phase-contrast microscopic images based on a combination of Otsu and watershed segmentation method. *Microscopy Research and Technique*, 1–12. <https://doi.org/10.1002/jemt.23893>